JOURNAL OF THERMOPHYSICS AND HEAT TRANSFER
Vol. 17, No. 4, October–December 2003

Technical Notes

TECHNICAL NOTES are short manuscripts describing new developments or important results of a preliminary nature. These Notes cannot exceed six manuscript pages and three figures; a page of text may be substituted for a figure and vice versa. After informal review by the editors, they may be published within a few months of the date of receipt. Style requirements are the same as for regular contributions (see inside back cover).

Experimental Thermal Contact Conductance of Bead-Blasted SS 304 at Light Loads

Fernando H. Milanez,* J. Richard Culham,† and M. Michael Yovanovich‡
University of Waterloo, Waterloo, Ontario N2L 3G1, Canada

Nomenclature

c_1	=	Vickers microhardness correlation coefficient, Pa
c_2	=	Vickers microhardness correlation coefficient
E	=	Young's modulus, Pa
H	=	microhardness, Pa
h_c	=	contact conductance, W/m$^2 \cdot$ K
k_s	=	harmonic mean thermal conductivity, $2k_Ak_B/(k_A + k_B)$, W/mK
m	=	combined mean absolute slope, $\sqrt{(m_A^2 + m_B^2)}$, rad
P	=	contact pressure, Pa
q	=	heat flux, W/m^2
T	=	temperature, K
ΔT	=	temperature drop, K
ν	=	Poisson's ratio
σ	=	combined rms roughness, $\sqrt{(\sigma_A^2 + \sigma_B^2)}$, m

Subscripts

A, B	=	contacting bodies
c	=	contact
v	=	Vickers microhardness

Introduction

CONTACT heat transfer has many applications in engineering, such as ball bearings, spacecraft thermal control, microelectronic chips, and nuclear fuel heat dissipation. Several models to predict thermal contact resistance/conductance are available in the literature. Sridhar and Yovanovich[1] presented an extensive survey of the most accepted thermal contact conductance models available. They compared the models against stainless steel (SS) 304, Ni 200, Al 6061, Zr–Nb, and Zr-4 data collected by other researchers and concluded that the Cooper et al.[2] plastic model and the Mikic[3] elastic model are accurate to predict the experimental data, especially for high contact pressures. At light contact pressures, the theoretical models tend to underpredict experiments. The main objective of this work is to verify the deviation between experiments and theory at light loads.

To compare experiments and elastic or plastic models, it is convenient to know what is the deformation mode experienced by the contacting asperities. Mikic[3] proposed an index to predict if the deformation is either elastic or plastic. According to the author, the deformation mode depends on the geometry of the asperities and the mechanical properties of the contacting solids and does not depend on the magnitude of the contact pressure. In this work, the deformation mode of the contacting asperities is tested experimentally by measuring the contact conductance both in ascending and descending levels of contact pressures. It is well known that when the deformation is plastic, the thermal contact conductance measured in descending levels of contact pressure is always larger than in ascending levels because of the hysteresis effect (Mikic,[4] McWaid,[5] and Li et al.,[6] among others). The plastic deformation generated during the first loading is not recovered during the unloading; therefore, the contact spots are larger than during the first loading.

Review of Thermal Contact Conductance Models

The Cooper et al.[2] plastic model and the Mikic[3] elastic model are used here. These models were developed for isotropic surfaces (such as bead blasted). Yovanovich,[7] presented the following simple correlation for the Cooper et al.[2] plastic model:

$$h_c\sigma/k_sm = 1.25(P/H_c)^{0.95} \tag{1}$$

where P/H_c, the dimensionless contact pressure, is computed using the model proposed by Song and Yovanovich[8]:

$$P/H_c = \left[P\Big/c_1(1.62\sigma/m)^{c_2}\right]^{1/(1+0.071c_2)} \tag{2}$$

Mikic[3] presented the following correlation for his elastic model:

$$h_c\sigma/k_sm = 1.55\left(\sqrt{2}P\Big/mE'\right)^{0.94} \tag{3}$$

where

$$E' = \left[\left(1-\upsilon_A^2\right)\Big/E_A + \left(1-\upsilon_B^2\right)\Big/E_B\right]^{-1} \tag{4}$$

is the effective Young's modulus of the contacting bodies (A and B).

Experimental Study

The experimental study consists of measuring the thermal contact conductance between two SS 304 specimens under vacuum environment. The two specimens are nominally flat, with one of the contacting specimens smooth (lapped) and the other rough (bead blasted). The experimental setup and procedure used here is basically the same as employed by other researchers (McWaid[5] and Li et al.,[6] among others). It consists basically of a cold plate, testing column (two contacting samples), load cell, electrical heater, and loading

Presented as Paper 2002-0787 at the AIAA 40th Aerospace Sciences Meeting, Reno, NV, 14–17 January 2002; received 21 February 2002; revision received 19 November 2002; accepted for publication 8 January 2003.

*Research Assistant, Microelectronics Heat Transfer Laboratory, Department of Mechanical Engineering; currently with Solar Energy Laboratory, Department of Mechanical Engineering, Federal University of Santa Catarina, 88040-900 Florianopolis SC, Brazil; milanez@labsolar.ufsc.br.

†Associate Professor and Director of Microelectronics Heat Transfer Laboratory, Department of Mechanical Engineering; rix@mhtlab.uwaterloo.ca.

‡Distinguished Professor Emeritus, Microelectronics Heat Transfer Laboratory, Department of Mechanical Engineering; mmyov@mhtlab.uwaterloo.ca. Fellow AIAA.

mechanism. Heat is dissipated in the electrical heater, crosses the test column, and is absorbed by the cold plate. The contact pressure is read by means of a load cell.

The temperature distribution of the testing column is measured by means of six number 36 type-T thermocouples positioned 5 mm apart from each other along the longitudinal direction in each sample. A computational code uses the least-square method to find the best linear fit for the temperature distribution inside each test specimen. The heat fluxes of each sample are obtained by multiplying the slope of the temperature distributions by the conductivity of the SS 304, which is a function of the temperature and is given by the following expression:

$$k_{SS304} = 10.05 + 0.028T, \qquad 277 < T < 360\ \text{K} \qquad (5)$$

This correlation was obtained in a previous conductivity test using calibrated ARMCO fluxmeters.

All four SS 304 specimens were machined from the same bar stock to cylinders of 25 mm diameter by 45 mm long. The specimens were then ground flat, lapped by means of a mechanical lapping machine, and further hand lapped to obtain maximum flatness. The flatness deviations of the lapped surfaces were checked using a monochromatic light source and an optical flat and did not exceed 0.5 μm. Two specimens remained flat, and the other two specimens were bead blasted to two different roughness levels (0.72 and 1.31 μm). The roughnesses were measured with a stylus profilometer both before and after the tests, and the differences were negligible. A Vickers microhardness test was performed on one of the flat specimens, and the Vickers microhardness correlation coefficients obtained using this procedure were $c_1 = 10.6$ GPa and $c_2 = -0.40$.

The test procedure consisted of assembling the testing pair (one flat lapped and one bead-blasted sample) inside the vacuum chamber. The chamber was closed, and a vacuum was drawn using a mechanical pump connected in series with a diffusion punp. The vacuum inside the chamber was 10^{-6} torr. The electrical heater was turned "on," and the system was left for at least 16 h to achieve steady state. The thermal contact conductance was computed by means of the following expression:

$$h_c = q/\Delta T \qquad (6)$$

where q is the average of the heat fluxes of the two contacting specimens. The temperature drop ΔT is computed by extrapolating the temperature profiles of each contacting specimen to the interface. For comparison between the experiment and theory, the thermal conductivity of SS 304 [k_s appearing in Eqs. (1) and (3)] is evaluated at the mean temperature of the contact, which is the average of the two extrapolated temperatures.

This procedure was repeated for each contact pressure level tested. The pressure levels varied from 15.8 to approximately 3000 kPa in both ascending and descending levels. Two loading/unloading cycles were measured for each pair. The system was considered to be in steady state when the thermal contact conductance between the specimens did not vary more than 1% in 1 h. As the contact pressure was increased between each pressure step, the power level of the electrical heater was increased to maintain a reasonable temperature drop (8–40°C) between the samples. The mean temperature of the interface ranged from 15 to 60°C.

For light contact pressures, the uncertainty of heat flux measurement is ±5%, and the uncertainty of the temperature drop across the interface is ±1%. When the methodology of error propagation[9] is used, the uncertainty of the thermal contact conductance measurements is ±5% for the lightest contact pressure. For the highest contact pressure, the uncertainties of the heat flux and of the temperature drop were both ±2%, and the thermal contact conductance uncertainty is also ±5%.

Experimental Results and Comparison with Theory

Figure 1a shows the results for the smoothest of the two pairs tested, $\sigma = 0.72$ μm. It can be clearly seen that the hysteresis loop appears during both the first and second loading/unloading cycles.

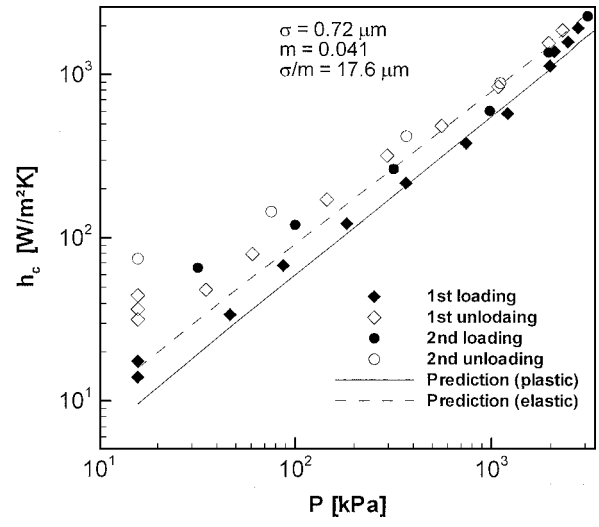

a)

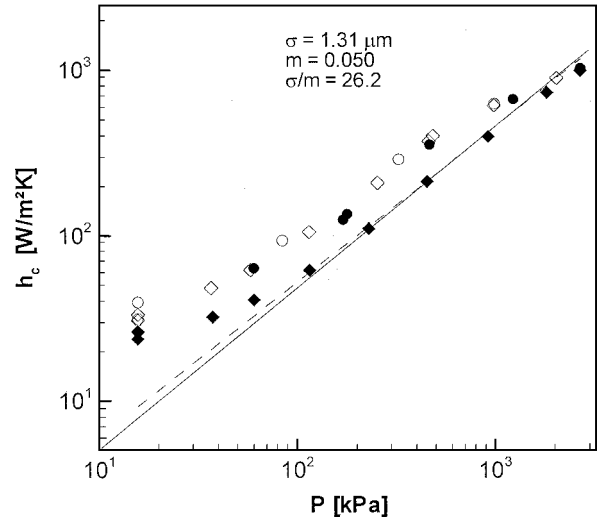

b)

Fig. 1 SS 304 bead-blasted/lapped contact conductance results.

The maximum difference between loading and unloading is 100% for the first cycle and 75% for the second cycle. Therefore, during both first and second loading/unloading cycles the asperities undergo plastic deformation. The comparison between the experimental results and the plastic model [Eq. (1)] for the first loading is reasonably good, especially for large contact pressures. At the lightest contact pressure, the plastic model underpredicts the first loading data by approximately 40%. The elastic model [Eq. (3)] predicts larger values of thermal contact conductance than the plastic model and is in fairly good agreement with the first unloading and the second loading/unloading cycle for high contact pressures despite that the asperities had already been plastically deformed during the first loading.

The results for the roughest test pair, $\sigma = 1.31$ μm, and the comparison against both the elastic and the plastic models are shown in Fig. 1b. The hysteresis loop is evident during the first loading/unloading cycle but not during the second cycle. The second loading/unloading cycle data points lie approximately over the same curve as the first unloading. These observations lead to the conclusion that the deformation is plastic during the first loading and elastic during the subsequent unloading/loading/unloading cycles. The plastic model predicts the first loading data very well for high contact pressures, similar to the smoother pair. For light contact pressures, the plastic model underpredicts the experimental data by a maximum difference of 70% for the lightest contact pressure.

The elastic and the plastic models predict similar values of contact conductance for this pair, and the elastic model predicts the first loading very well, especially at high contact pressures. However, the appearance of the hysteresis loop clearly shows that the deformation is plastic during the first loading. If one simply compares first loading data with the elastic model, the good agreement could suggest that the deformation of the asperities is elastic, which is not true. On the other hand, when a complete loading/unloading cycle is measured, it is easy to verify that the deformation mode of the contacting asperities is plastic in this case. The data points for first unloading and second loading/unloading cycle lie well above the models, as expected, due to the plastic deformation experienced by the asperities during first loading.

The plastic model presents the same behavior when compared with both test pairs: For the first loading, it underpredicts the experimental data at light loads, but as the pressure increases, the theoretical prediction gets closer to the measured values. This observation is in agreement with the experimental data compiled by Sridhar and Yovanovich.[1] Because this phenomenon has been consistently detected by different researchers employing different setups, it does not seem to be a weakness of the experimental program adopted here. The present authors believe that this is a weakness of the theoretical models. The theoretical models assume a Gaussian asperity height distribution, but the authors believe that the highest asperities of the real surfaces are truncated. At light contact pressures, only the higher asperities come into contact, and the truncation of the highest asperities makes the mean separation between the contacting surfaces smaller than predicted by the Gaussian model. Because the actual separation is smaller than predicted, the actual thermal contact conductance is higher than predicted by the Gaussian model, especially at light contact pressures. As the contact pressure increases, more and more asperities come into contact, and the effect of the few truncated asperities becomes negligible. A new thermal contact conductance model that takes the effect of the truncation of the contacting asperities into account is needed.

Conclusions

The appearance of the hysteresis loop indicated that the contact between bead-blasted/lapped SS 304 is plastic during the first loading/unloading cycle for both roughness levels tested, 0.72 and 1.31 μm. The plastic model of Cooper et al.[2] predicted first loading data points very well for high contact pressures. For light contact pressures, the model underpredicts the experiments. Other researchers employing different experimental setups have systematically noticed this unexpected behavior, indicating that this is a weakness of the theoretical models. The present authors believe that the models underpredict the experiments at light loads due to the truncation of the highest asperities; the highest asperities are shorter than predicted by the models. A new model is needed for the light contact pressure range.

Acknowledgments

F. H. Milanez acknowledges the Brazilian Federal Agency for Post-Graduate Education (CAPES) for supporting this project. J. R. Culham and M. M. Yovanovich acknowledge the financial support of the Natural Sciences and Engineering Research Council of Canada.

References

[1]Sridhar, M. R., and Yovanovich, M. M., "Review of Elastic and Plastic Contact Conductance Models: Comparison with Experiment," *Journal of Thermophysics and Heat Transfer*, Vol. 8, No. 4, 1994, pp. 633–640.

[2]Cooper, M., Mikic, B., and Yovanovich, M. M., "Thermal Contact Conductance," *Journal of Heat and Mass Transfer*, Vol. 12, 1969, pp. 279–300.

[3]Mikic, B. B., "Thermal Contact Conductance; Theoretical Considerations," *Journal of Heat and Mass Transfer*, Vol. 17, 1974, pp. 205–214.

[4]Mikic, B. B., "Analytical Studies of Contact of Nominally Flat Surfaces; Effect of Previous Loading," *Journal of Lubrication Technology*, Vol. 20, Oct. 1971, pp. 451–456.

[5]McWaid, T. H., "Thermal Contact Resistance Across Pressed Metal Contact in a Vacuum Environment," Ph. D. Dissertation, Mechanical Engineering Dept., Univ. of California, Santa Barbara, CA, Sept. 1990.

[6]Li, Y. Z., Madhusudana, C. V., and Leonardi, E., "On the Enhancement of the Thermal Contact Conductance: Effect of Loading History," *Journal of Heat Transfer*, Vol. 122, Feb. 2000, pp. 46–49.

[7]Yovanovich, M. M., "Thermal Contact Correlations," *Spacecraft Radiative Heat Transfer and Temperature Control*, edited by T. E. Horton, Vol. 83, Progress in Astronautics and Aeronautics, AIAA, New York, 1981, pp. 83–95.

[8]Song, S., and Yovanovich, M. M., "Relative Contact Pressure: Dependence on Surface Roughness and Vickers Microhardness," *Journal of Thermophysics and Heat Transfer*, Vol. 2, No. 4, 1988, pp. 633–640.

[9]Holman, J. P., *Experimental Methods for Engineers*, 6th ed., McGraw–Hill, Singapore, 1994, pp. 49–51.

Cooling Fin Design

V. Bertola*
Ecole Normale Supérieure, 75005 Paris, France
and
E. Cafaro†
Politecnico di Torino, 10129 Turin, Italy

Nomenclature

A	=	area of the fin cross section, m^2
b	=	q/kT_a, m^{-1}
h	=	heat transfer coefficient, W/Km^2
L	=	fin length, m
k	=	thermal conductivity, W/Km
m	=	fin parameter, m^{-1}
P	=	perimeter of the fin cross section, m
q	=	heat flux at the fin root, W/m^2
T	=	fin temperature, K
T_a	=	ambient temperature, K
T_L	=	tip temperature, K
T_0	=	temperature at the fin root, K
x	=	dimensionless position along the fin
z	=	position along the fin, m
θ	=	dimensionless temperature, $(T - T_a)/T_a$
θ_L	=	dimensionless temperature at the tip, $(T_L - T_a)/T_a$
θ_0	=	dimensionless temperature at the fin root, $(T_0 - T_a)/T_a$

Introduction

RECENT advances in high-performance designs for everything from electronic components at the submicron scale to equipment used in aircraft and space vehicles have increased the need for enhanced heat transfer devices. The design and analysis of fin structures for extended surface heat transfer are at the forefront of this technology. Although the basics of the heat conduction process in straight fins are extensively discussed in standard heat transfer textbooks,[1] the design of specific applications often requires a more detailed analysis leading to a broad range of surface types and operating conditions.[2]

Received 15 May 2002; revision received 12 June 2003; accepted for publication 12 June 2003.

*Research Associate, Laboratoire de Physique Statistique, 24 Rue Lhomond.

†Associate Professor, Dipartimento di Energetica, Corso Duca degli Abruzzi 24.

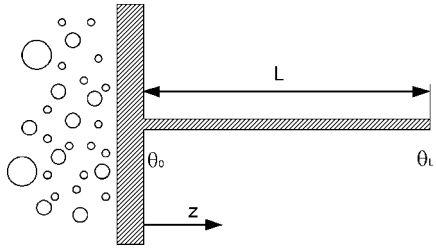

Fig. 1 Schematic representation of a fin cross section; the boundary condition at the fin root is imposed by a fluid undergoing a gas–liquid phase transition.

The solution of any heat conduction problem in a cooling fin is given by the differential equation[1]

$$\frac{\mathrm{d}^2(T-T_a)}{\mathrm{d}z^2} = \frac{hP}{kA}(T-T_a) \tag{1}$$

where A and P account for the geometry of the fin cross section. The solution of this equation represents the temperature distribution along the fin for selected initial and boundary conditions.

An interesting one-dimensional, steady-state problem of heat conduction arises in designing a cooling fin with fixed temperature boundary conditions at both ends and specified heat flux at the root. This set of conditions can be realized if the fin is connected to a wall where a phase change occurs, as is schematically depicted in Fig. 1. Whereas from the purely mathematical standpoint the direction of the heat flux is not important, in practical applications the flux is always directed from the fluid to the fin; that is, the fin is used to dissipate thermal energy transported by the fluid. This happens when a vapor flow undergoes homogeneous condensation or when a liquid flow starts boiling due to internal heat sources (for instance, chemical or nuclear reactions). The latter circumstance is notably important, because it is a typical consequence of an accident, and the cooling fin must act as a passive safety device, dissipating the unwanted excess heat.

In such cases, the heat flux at the fin root may change considerably while the wall temperature is almost constant.[3] Thus, the second-order heat equation must satisfy three boundary conditions so that an additional degree of freedom must be introduced in order to achieve a well-posed problem. For instance, a natural choice is to consider the fin length as a variable. In this Note the analytical solution of this problem is discussed as a function of the heat flux. A numerical example is also presented. The results indicate that, depending on the value of the heat flux at the fin root, the problem of heat conduction in a fin of variable length may have no solutions, one solution, or two solutions.

Analysis

The steady-state, dimensionless conductive problem for the fin is as follows:

$$\ddot{\theta}(x) = (Lm)^2\theta(x), \qquad \dot{\theta}(0) = -Lb, \qquad \theta(0) = (T_0 - T_a)/T_a$$

$$\theta(1) = (T_L - T_a)/T_a, \qquad 0 \le x \le 1 \tag{2}$$

where $x = z/L$, $m^2 = hP/kA$, and $b = q/kT_a$.

The solution that satisfies the differential equation and the boundary conditions at the fin root ($x = 0$) is

$$\theta(x) = (\theta_0 - b/m)\cosh(Lmx) + (b/m)e^{-Lmx} \tag{3}$$

The boundary condition at the tip allows one to derive a quadratic in e^{mL},

$$(\theta_0 - b/m)e^{2mL} - 2\theta_L e^{mL} + (\theta_0 + b/m) = 0 \tag{4}$$

that can be used to calculate the fin length. The solutions of Eq. (4) must be real and positive to represent a physical length. In particular, if $b = m\theta_0$ the one positive solution is

$$L = (1/m)\,\ell n(\theta_0/\theta_L) \tag{5}$$

whereas if $b \neq m\theta_0$ the solution is

$$e^{mL} = \frac{\theta_L \pm \sqrt{\theta_L^2 - \theta_0^2 + (b/m)^2}}{\theta_0 - (b/m)} \tag{6}$$

so that no real solutions exist if $b < m\sqrt{(\theta_0^2 - \theta_L^2)}$. Positive solutions for the fin length are obtained if the right-hand side of Eq. (6) exceeds unity, requiring

$$\frac{\theta_L - \theta_0 + (b/m) \pm \sqrt{\theta_L^2 - \theta_0^2 + (b/m)^2}}{\theta_0 - (b/m)} > 0 \tag{7}$$

Suppose first that $b > m\theta_0$ holds. The largest root corresponds to the plus sign, and Eq. (7) is physically realizable if

$$\sqrt{\theta_L^2 - \theta_0^2 + (b/m)^2} < \theta_0 - \theta_L - b/m \tag{8}$$

Squaring both sides leads to the contradiction $b < m\theta_0$.

On the other hand, the smallest solution gives

$$\sqrt{\theta_L^2 - \theta_0^2 + (b/m)^2} > \theta_L - \theta_0 + b/m \tag{9}$$

which is always true for $b > m\theta_0$; thus, there is one positive solution for the fin length if $b > m\theta_0$.

Suppose next that $b < m\theta_0$. Equation (7) with the plus sign gives the condition

$$\sqrt{\theta_L^2 - \theta_0^2 + (b/m)^2} > \theta_0 - \theta_L - b/m \tag{10}$$

which is always true for $b < m\theta_0$, whereas the minus sign gives the condition

$$\sqrt{\theta_L^2 - \theta_0^2 + (b/m)^2} < \theta_L - \theta_0 + b/m \tag{11}$$

which for $b < m\theta_0$ is always true as well. Thus, in this case there are two solutions. In conclusion, we have no solution for $b < m\sqrt{(\theta_0^2 - \theta_L^2)}$, one solution for $b \ge m\theta_0$, and two solutions for $m\sqrt{(\theta_0^2 - \theta_L^2)} < b < m\theta_0$.

Example

Consider a cylindrical fin attached to a wall where a water flow undergoing a liquid-to-gas phase change at atmospheric pressure occurs and suppose the phase transition is due to some undesired internal heat generation that must be removed by the fin. The temperature at the fin root is 373 K due to the phase change. Suppose that the temperature of the tip must be 323 K, and the temperature of the environment surrounding the fin is 293 K, so that $\theta_0 = 0.273$ and $\theta_L = 0.102$. For simplicity, let $m = 1$.

Values of the fin length as a function of the parameter b are shown in Fig. 2. For $b < 0.2532\ \mathrm{m}^{-1}$ there are complex solutions, whereas for $0.2532\ \mathrm{m}^{-1} < b < 0.273\ \mathrm{m}^{-1}$ there are two real solutions, and for $b > 0.273\mathrm{m}^{-1}$ one real solution; the largest solution becomes asymptotically infinite for $b = 0.273\ \mathrm{m}^{-1}$. The value of the heat flux in real applications, of course, must be smaller than the critical heat flux value, at which wall burnout would occur.[4] Although an infinite length of the fin is of no use for practical applications, the existence of two finite values of the fin length in a given range of heat fluxes provides an additional design parameter that could be exploited under particular circumstances. The same situation is depicted from a different standpoint in Fig. 3, which shows the values of the dimensionless temperature of the tip with respect to the fin length.

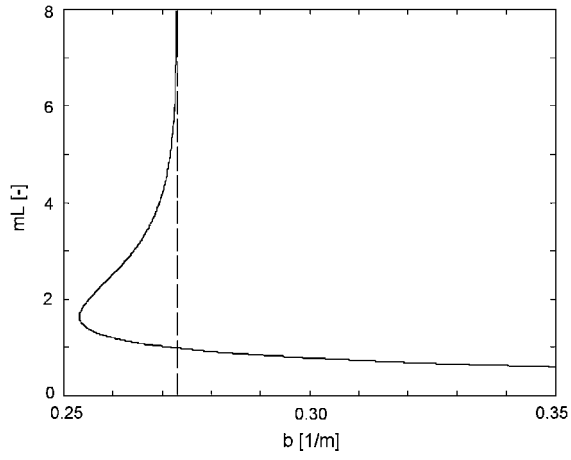

Fig. 2 Values of the total dimensionless fin length *mL* satisfying all of the boundary conditions, as a function of the parameter *b*, proportional to the heat flux at the fin root.

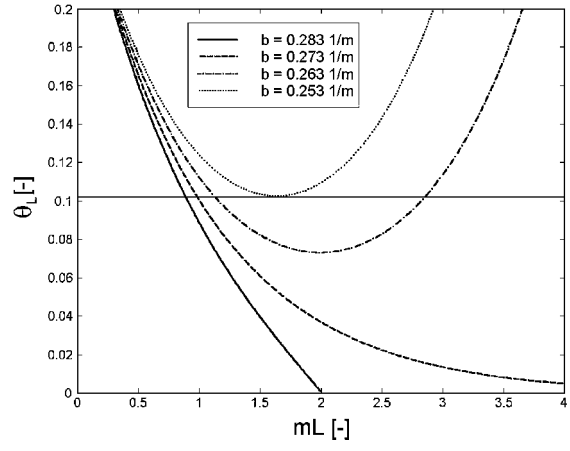

Fig. 3 Admissible values of the dimensionless temperature at the tip as a function of the fin length for different values of the parameter *b*; the solution of the problem is given by the intersection of the curves with the horizontal line at $\theta_L = 0.102$.

Conclusions

Although the heat conduction problem in cooling fins is usually considered to have one steady-state solution for given boundary conditions, two solutions may exist when nonstandard, yet physically admissible, boundary conditions are applied. In particular, the situation in which the cooling fin has fixed temperature at both ends and specified heat flux at the root is examined. The analysis shows that, depending on the value of the heat flux at the fin root, the problem may have no solutions, one solution, or two solutions for the fin length. The results can find practical applications in the design of passive safety devices for chemical or nuclear plants.

Acknowledgments

Laboratoire de Physique Statistique de l'Ecole Normale Supérieure is Unité Mixte de Recherche 8550 of the Centre National de la Recherche Scientifique, associated with the Universities Paris VI and Paris VII.

References

[1]Incropera, F. P., and De Witt, D. P., *Fundamentals of Heat and Mass Transfer*, Wiley, New York, 1990, p. 119.

[2]Kraus, A. D., Azziz, A., and Welty, J. R., *Extended Surface Heat Transfer*, Wiley, New York, 2001.

[3]Jens, W. H., and Lottes, P. A., "Analysis of Heat Transfer, Burnout, Pressure Drop, and Density Data for High Pressure Water," U.S. Dept. of Energy, U.S. Army Environmental Center Rept. ANL-4627, Argonne, IL, 1951.

[4]Celata, G. P., and Mariani, A., "Critical Heat Flux, Post-CHF Heat Transfer and Their Augmentation," *Modelling and Experimentation in Two-Phase Flows*, edited by V. Bertola, CISM Courses and Lectures, No. 450, Springer Wien New York, Vienna, 2003, Chap. 7.

Integral Equation for the Heat Transfer with the Moving Boundary

Vladimir V. Kulish*
Nanyang Technological University, Singapore 639798, Republic of Singapore
and
Vasily B. Novozhilov†
University of Ulster, Newtownabbey, England BT37 0QB, United Kingdom

Nomenclature

A	=	heated surface area, m^2
b	=	mean of normal distribution, s
c_p	=	specific heat of solid material
E	=	activation energy, J
F	=	fluence of the laser, J
K	=	preexponent
k	=	thermal conductivity, W m^{-1} K^{-1}
p	=	pressure, Pa
q''	=	local heat flux, W m^{-2}
q''_s	=	surface heat flux (at $x = 0$), W m^{-2}
R	=	gas constant
r	=	reflectivity of the material
T	=	absolute temperature, K
$T_{\max}$	=	maximum temperature during heating, K
T_s	=	surface temperature (at $x = 0$), K
T_0	=	initial temperature (at $t \leq 0$), K
t	=	time, s
u	=	speed of the domain boundary, m s^{-1}
x	=	coordinate normal to material surface, m
α	=	thermal diffusivity, m^2 s^{-1}
θ	=	excess temperature, $= T - T_0$, K
ϑ	=	normalized nondimensional temperature, $= (T_s - T_0)/(T_m - T_0)$
μ, ν	=	given parameters for a particular fuel
ρ	=	density, kg m^{-3}
σ	=	variance of normal distribution, s

Introduction

PROBLEMS of heat transfer in domains with moving boundaries are commonly found in scientific and engineering applications. As typical examples, one can consider the following classes of problems:

1) Stefan-type and related problems. These typically arise when there is a phase change at the boundaries between media with different conducting properties, for example, during melting/solidification of alloys or warming/freezing of water-containing soils.

Received 9 June 2003; revision received 29 July 2003; accepted for publication 30 July 2003.

*Associate Professor, School of Mechanical and Production Engineering, 50 Nanyang Avenue; mvvkulish@ntu.edu.sg or kulishv@asme.org.

†Professor, Faculty of Engineering and Built Environment, Jordanstown Campus, Shore Road.

2) Evaporation of liquid layers and droplets under external heat flux conditions.

3) Combustion of solids and liquids, which cause fuel surface regression. This phenomenon occurs, for example, during pool and tank fires, as well as for burning plastics and solid propellants.

A convenient and effective way of solving such problems is reduction to the sets of integral or integro–differential equations, containing unknown properties at boundary locations. The primary importance of such methods is due to the removal of unnecessary numerical complications (such as adjustment of the grid to moving boundaries, grid refinement in the regions of sharp gradients, necessity to make grid refinement tests, etc.).

In the present Note, a relationship between the local temperature and the heat flux, obtained earlier for a semi-infinite conducting solid,[1] is expanded to the case of the domain with a moving boundary. The obtained relationship leads to an integral equation at the moving boundary, which can be used for convenient calculation of the surface temperature.

Solution of the Problem

Consider a one-dimensional semi-infinite domain whose boundary is moving with a constant velocity u. This domain is initially, at time $t = 0$, in thermal equilibrium with the temperature $T = T_0$. The surface heating of the domain starts at time $t = 0$, and the value of heat flux is $q_s''(t)$.

In this case, the energy equation assumes the form

$$\frac{\partial T}{\partial t} + u\frac{\partial T}{\partial x} = \alpha\frac{\partial^2 T}{\partial x^2} \tag{1}$$

where α is the domain thermal diffusivity.

After introducing the excess temperature, defined as $\theta = T - T_0$, and a new "spatial" variable, $\xi = x/\sqrt{\alpha}$, the solution to Eq. (1) can be found by using the Laplace transform technique (see Ref. 1 for details). The solution is in the form of an integral equation that relates temperature and heat flux, namely,

$$T(x,t) = T_0 + \int_0^t q''(x,\tau)\left[\frac{e^{(-u^2/4\alpha)(t-\tau)}}{\sqrt{\pi k\rho c_p(t-\tau)}} + \frac{u}{2k}\operatorname{erfc}\left(-\frac{u}{2}\sqrt{\frac{t-\tau}{\alpha}}\right)\right]d\tau \tag{2}$$

Equation (2) provides one with the relationship between the local values of temperature and heat flux and is true everywhere in a one-dimensional semi-infinite domain whose boundary is moving with a constant velocity. It is noteworthy to emphasize here that the relationship given by Eq. (2) is valid everywhere, including the domain boundary. Thus, the surface temperature $T_s(t)$ of the domain under consideration can be found for a given surface heat flux $q_s''(t)$ as

$$T_s(t) = T_0 + \int_0^t q_s''(\tau)\left[\frac{e^{(-u^2/4\alpha)(t-\tau)}}{\sqrt{\pi k\rho c_p(t-\tau)}} + \frac{u}{2k}\operatorname{erfc}\left(-\frac{u}{2}\sqrt{\frac{t-\tau}{\alpha}}\right)\right]d\tau \tag{3}$$

Observe also from Eq. (2) that if the domain boundary is at rest, that is, $u = 0$, then the solution becomes

$$T(x,t) = T_0 + \int_0^t \frac{q''(x,\tau)}{\sqrt{\pi k\rho c_p(t-\tau)}}\,d\tau \tag{4a}$$

which, on the other hand, can be written in terms of fractional (of noninteger order) derivatives as

$$T_s(t) = T_0 + \frac{1}{\sqrt{k\rho c_p}}\frac{\partial^{-\frac{1}{2}} q''(x,t)}{\partial t^{-\frac{1}{2}}} \tag{4b}$$

the result that was reported in Ref. 1.

Physical Interpretation

As one example of physical interpretation of the solutions (2) and (3), consider combustion of a uniform solid propellant, described by Eq. (1). It is well known[2] that the surface temperature of the propellant may vary with time, and consideration of this effect is quite important in real applications.

The linear regression rate of the propellant's surface, u, depends on a number of external factors, such as pressure in the combustion chamber, as well as on the properties of the fuel itself. Different correlations have been proposed to describe burning rates of solid propellants. Typical models[2] assume linear burning rate in the form

$$u = K\rho^{-1}p^{\nu}T_s^{\mu}\exp[-E/(2RT_s)] \tag{5}$$

In this relationship, both surface temperature and pressure are generally functions of time.

It is apparent from Eq. (5) that the constant burning rate u occurs when the gas pressure in the combustion chamber varies with time as

$$p(t) = \left(\text{const}\cdot K^{-1}\rho[T_s(t)]^{-\mu}\exp\{E/[2RT_s(t)]\}\right)^{1/\nu} \tag{6}$$

One can also consider this example as a combustion control problem. For stability of combustion and good rocket engine performance, it is usually desirable to achieve steady-state regimes of burning. Under such a set of the problem, the external heat flux $q_s''(t)$ and the chamber pressure $p(t)$ can be viewed as controlling parameters, which can be varied with time in order to achieve the required rate of burning. The heat flux and pressure would control fuel conditions, such as surface temperature and burning rate. The required control function $[q_s''(t),\ p(t)]$ can be found using Eqs. (3) and (6).

Numerical Simulation

The solution for the surface temperature, given by Eq. (3), was tested by numerically solving several cases implying different sets of boundary data for the heat flux.

To be consistent with the results obtained previously, the physical properties of a GaAs bulk sample ($r = 0.39$, $\rho c_p = 1.73\ 10^6$ J/m^{3}K, $k = 52$ W m^{-1} K^{-1}) were used in the course of the numerical simulation (see Ref. 3 for details).

First, the surface temperature was computed in the case of a constant heat flux value, $q_s'' = 10^3$ W m^{-2}, for three different values of the boundary speed u: 0, 1.0, and 10.0 m s^{-1}, respectively. The results are shown in Fig. 1.

Although at the same time the absolute values of the surface temperature are different for different values of the boundary speed, the surface temperature behavior follows $T_s(t) \sim \sqrt{t}$, which indeed must be the case for a constant value of the surface heat flux. Moreover, the result, in the case of zero boundary speed, matches the result reported in Ref. 1 for the same case [see Eq. (4)].

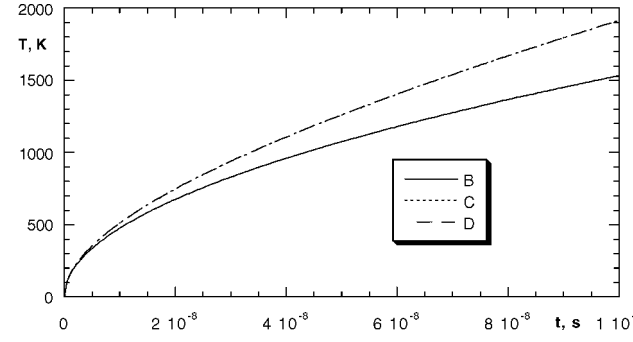

Fig. 1 Time evolution of the surface temperature in the case of a constant heat flux: B, zero boundary speed; C, boundary speed 1.0 m s^{-1}; and D, boundary speed 10.0 m s^{-1}.

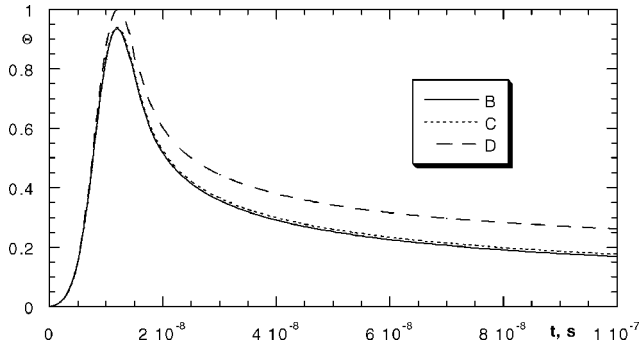

Fig. 2 Time evolution of the surface temperature in the case of a pulsing heat flux: B, zero boundary speed; C, boundary speed 1.0 m s^{-1}; and D, boundary speed 10.0 m s^{-1}.

The next case, computed numerically, was a simulation of the fast laser heating of the surface. The surface heat flux was given by the Gaussian distribution, in exactly the same manner as it was done in Ref. 3, that is,

$$q_s''(t) = \frac{F(1-r)}{2A\sigma\sqrt{\pi}} \exp\left[-\left(\frac{t-b}{\sigma}\right)^2\right] \tag{7}$$

This situation mimics a pulsed Nd:YAG laser radiating at 532-nm wavelength used as a heating source, with a fluence F that can be set from 0 to 1.0 mJ. The parameters of the laser pulse were chosen in order to be consistent with the results reported in Ref. 3.

The numerical results, representing the time evolution of the dimensionless excess surface temperature, $\theta = (T - T_0)/(T_{\max} - T_0)$, are shown in Fig. 2 for three different values of the boundary speed u:0, 1.0, and 10.0 m s^{-1}.

The solution represented by curve B (zero speed of the boundary) coincides with the solution reported in Ref. 3 and given by Eq. (4).

Conclusions

Using the same method that was initially proposed in Ref. 1, the relationship between the local temperature and local heat flux has been established for the homogeneous one-dimensional heat equation in a semi-infinite domain whose boundary moves with a constant velocity. This relationship has been written in the form of a convolution integral.

The integral equation, relating the surface temperature and surface heat flux, has been solved numerically in the case of a constant heat flux value and in the case of a pulsing heat flux, mimicking fast laser heating of solid materials.

The results obtained in the course of the numerical simulation show the following:

1) These results coincide with those results obtained by the same method in the case of a nonmoving boundary.

2) The value of the boundary speed influences the surface temperature value—if the former increases, the latter increases too—but not the shape of the time evolution curve.

3) The moving boundary effect is not very significant in the case of fast laser heating due to the shortness of the process.

References

[1]Kulish, V. V., and Lage, J. L., "Fractional-Diffusion Solutions for Transient Local Temperature and Heat Flux," *Journal of Heat Transfer*, Vol. 122, No. 2, 2000, pp. 372–376.

[2]Novozhilov, B. V., *Unsteady Combustion of Solid Propellants*, Nauka, Moscow, 1973.

[3]Kulish, V. V., Lage, J. L., Komarov, P. L., and Raad, P. E., "Fractional-Diffusion Theory for Calculating Thermal Properties of Thin Films from Surface Transient Thermoreflectance Measurements," *Journal of Heat Transfer*, Vol. 123, Dec. 2001, pp. 1133–1138.

Thermal Conductance Across Oxygen-Free High-Conductivity Copper Contacts in Different Environments

Bapurao Kshirsagar,* J. Nagaraju,† and M. V. Krishna Murthy‡
Indian Institute of Science, Banglaore 560 012, India

Nomenclature

A_c	=	apparent contact area
H_c	=	microhardness of contacting surface
h_c	=	thermal contact conductance
h_g	=	gap conductance
k	=	thermal conductivity
m	=	average asperity slope
P	=	contact pressure
Q	=	heat flow rate
σ	=	rms value of surface roughness

Introduction

WHEN two metallic surfaces are brought into contact to transmit heat, the uniform flow of heat is restricted to conduction through the contact spots, which are limited in number and size. The magnitude of contact conductance is a function of a number of parameters including the thermophysical and mechanical properties of the materials in contact, the characteristics of the contacting surfaces, the presence of interstitial media, the contact pressure, the mean interface temperature, and the conditions surrounding the contact. Fletcher[1] reviewed the various experimental techniques to measure the thermal contact resistance. Mikic[2] investigated theoretically the effect of mode of deformation on the predicted values of thermal contact conductance and suggested a correlation for both plastic and elastic deformations. Sridhar and Yovanovich[3] proposed an elastoplastic contact–conductance model for isotropic and conforming rough surfaces. Wahid and Madhusudana[4] gave a relation between the effective gap thickness and surface roughness for all gases. In view of the significant number of parameters affecting the thermal contact conductance, it is mostly determined experimentally to provide a measure of the thermal performance of a specific configuration. The objective of the present investigation is to study the variation in thermal conductance across oxygen-free high-conductivity(OFHC) copper contacts in vacuum, nitrogen, and helium environments.

Experimentation

A schematic of the thermal contact conductance measurement test setup is shown in Fig 1. It consists of a contact conductance cell, a hydraulic loading unit, a heating circuit, a cooling circuit, a vacuum system, and instrumentation. The test column assembly consists of a pair of heater–cooler blocks, test specimens, heat-flux meters made of OFHC copper, and a pair of ball-cone seat arrangement on either side. The heater–cooler block can be used either as a heater or as a cooler. A triple-walled chamber made of AISI304 accommodates

Received 18 September 2002; revision received 26 March 2003; accepted for publication 21 April 2003.

*Research Student, Department of Instrumentation.
†Assistant Professor, Department of Instrumentation.
‡Professor, Department of Instrumentation.

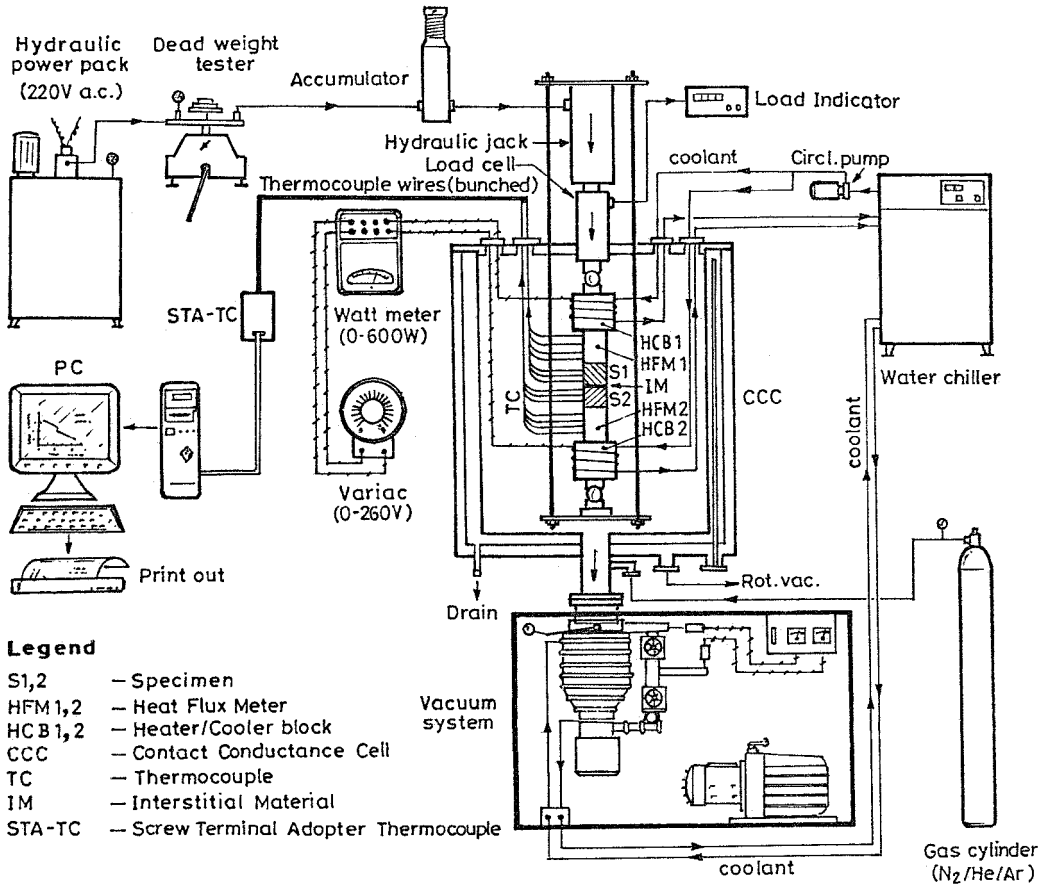

Fig. 1 Experimental setup.

the test column and is designed to withstand a vacuum of 5×10^{-6} torr. The loading system consists of a hydraulic power pack, a dead-weight tester, a hydraulic jack, a compression-type load cell, a digital load indicator, a loading pin, the test column, and a triangular frame to apply load gradually on the test column. The load is transmitted to the contacting specimens through stainless-steel ball bearings to provide an axial load. Load is measured with a load cell, which is precalibrated over the load range of interest by dead-weight method. The entire test facility is enclosed in a vacuum chamber, which is held at vacuum level of 10^{-5} torr to minimize convective heat losses from the cylindrical surfaces of the heat-flux meters. A passive radiation shield consisting of a highly reflective aluminum foil surrounds the test column. The system is equipped with the necessary instruments like electrical wattmeter, vacuum gauges, data-acquisition system, etc., for the measurement of various parameters. The heat-flux meters made of OFHC copper (25-mm diam and 50-mm height) are used for measuring the heat flow rate through the test column. The heat flow rate is calculated from the temperature gradient along the heat-flux meter and its thermal conductivity (from the manufacturer's data, $k = 384$ W/mK). Zirconium oxide discs are used at the end of the source and the sink to prevent heat loss by conduction. Thermal grease is applied to all of the interfaces except for the test interfaces in order to enhance the heat transfer. The specimens and the heat-flux meters are inserted in a Teflon® tube for aligning them axially and also to reduce the radial heat losses. Thermocouples (T-type, 24SWG) are fixed in 1-mm-diam holes drilled on the test specimens and the heat-flux meters with a heat sink compound. These thermocouples are calibrated with Physikalische Technische Bundesansatt certified secondary standard thermometer set. All thermocouple ends are terminated at a junction box, which is connected to a DASTC/B (Keithley) 16-channel thermocouple data logger card (interfaced to a PC) through an interface cable. This will automatically log the temperature data onto the files.

The cylindrical-shaped specimens of 25-mm length and 25-mm diam are prepared from the same OFHC copper. One end surface of each of these specimen surfaces is subjected to different machining operations, namely, turning and grinding, lapping with different silicon-carbide compounds and polishing with an emery cloth (spread over a flat glass surface) of different grit sizes. The specimen surfaces are cleaned in an ultrasonic bath to remove the dirt, and they are further cleaned with acetone and then with isopropyl alcohol. The surface characteristics (σ and m) are measured using a form Talysurf series-5 (Taylor Hobson), and the microhardness H_c is measured using a microhardness tester (HMV 2000 Shimadzu). The measured values are

$$\sigma = 0.155\ \mu\text{m}, \qquad m = 0.003, \qquad H_c = 1393\ \text{MPa}$$

The hydraulic system is switched on, and a certain pressure is applied on the test column before the chamber is evacuated. The input heat is adjusted to set the desired thermal gradient along the test column. The entire system is kept on for 12 h so that it reaches a steady state. This steady-state temperature values are recorded for every load and are used to determine the temperature gradients in the test specimens. Then the heater current is increased to a higher value, and the measurements are repeated. The heat-flux values in the heat-flux meters can be calculated using the temperature gradient obtained by a linear least-squares fit and the thermal conductivity of the heat-flux meter material. For all heat inputs the heat-flux values obtained from the two-heat flux meters differed by less than 3%. This shows that the heat flow in the test column is nearly one-dimensional and the radial heat losses are negligible. Thermal contact conductance is given by $h_c = Q/(A_c \Delta T)$, where ΔT is the temperature drop across the interface. This is obtained by extrapolating the source-side and sink-side specimen temperature profiles. The accuracy in temperature measurement is ± 0.2°C, and the uncertainty in heat flow rate Q measurement is $\pm 2.5\%$. Experiments were conducted across OFHC copper contacts by varying the contact pressure (1–12 MPa) across the interface in vacuum, nitrogen, and helium.

Results and Discussion

The results obtained on interface temperature drop and heat flow rate are used to calculate the thermal contact conductance. Figure 2 shows the variation of thermal contact conductance with contact pressure. Extrapolation of the curve to zero-contact pressure did not approach zero-contact conductance value, but a finite value. When the load is minimum or even when the load is fully removed, the specimens will always be touching each other at some contact points because of self-weight and will contribute to some amount of heat transfer across the contact. The variation of thermal contact conductance with contact pressure in nitrogen and helium is also compared with vacuum in the same Fig. 2. Thermal contact conductance increases with the introduction of gas (either nitrogen or helium). The gas molecules occupy the voids between the contacting surfaces and help to conduct some more heat between contacting surfaces. This heat transfer depends on many parameters like thermal conductivity of gas itself, thermal conductivity of contacting surfaces, gap distance, etc. Convective heat transfer in the gap is negligible as gap distance is very small. Because the mean interface temperature is low, the heat transfer by radiation is negligible. Therefore, the heat transfer at the gap can be considered to be purely by conduction. Thermal conductance in helium environment is higher than in nitrogen because its thermal conductivity (0.15 W/mK) is six times higher than that of nitrogen (0.0258 W/mK). Thermal conductance also increases with contact pressure.

Mikic[2] suggested the following equation to calculate theoretically the contact conductance h_c across metallic contacts in vacuum:

$$h_c = 1.13k(m/\sigma)(P/H_c)^{0.94} \qquad \text{W/m}^2\text{K}$$

Yovanovich et al.[5] modified the preceding expression as

$$h_c = 1.25k(m/\sigma)(P/H_c)^{0.95} \qquad \text{W/m}^2\text{K}$$

Using the preceding two theoretical models, thermal contact conductance h_c of OFHC copper contacts is calculated at different contact pressures. These values are compared with the present experimental values in Fig. 2. It shows that the measured values of thermal contact conductance in vacuum are in good agreement with the theoretical models.

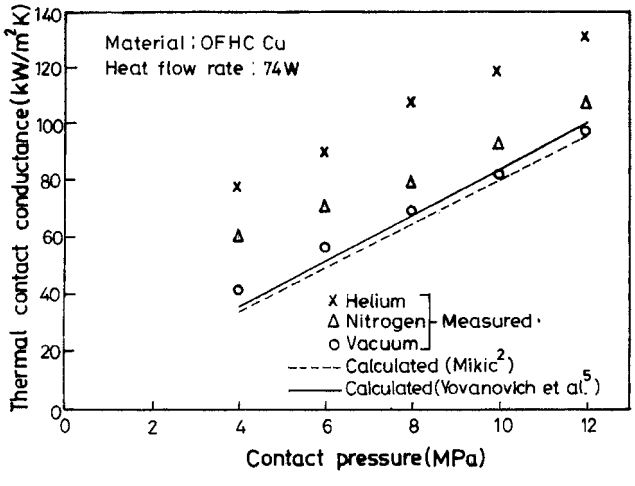

Fig. 2 Variation of thermal contact conductance with contact pressure.

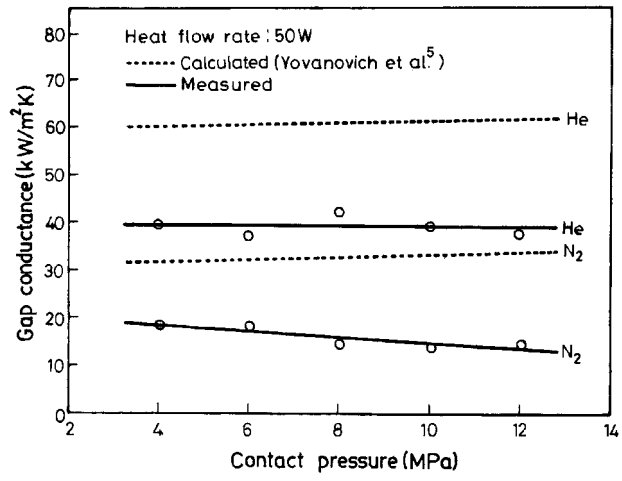

Fig. 3 Variation of gap conductance with contact pressure.

The gap conductance is calculated as per the procedure given by Yovanovich et al.[5] Thus the data obtained in nitrogen and helium environments are compared in Fig. 3 with the experimental data. Though the gap conductance in both the media shows the same trend as that predicted by Yovanovich et al.,[5] the model is not adequate for prediction.

Conclusions

Thermal conductance varies not only with the contact pressure but also with the thermal conductivity of interstitial gas media. The present theoretical models are not adequate for predicting the gap conductance across metallic contacts when their gap is filled with a gas.

References

[1] Fletcher, L. S., "Experimental Techniques for Thermal Contact Resistance Measurements," *Experimental Heat Transfer, Fluid Mechanics and Thernodynamics*, edited by M. D. Kelleher, K. R. Srinivasan, R. K. Shah, and Y. Joshi, Elsevier Science, New York, 1993.

[2] Mikic, B. B., "Thermal Contact Conductance Theoretical Consideration," *International Journal of Heat and Mass Transfer*, Vol. 17, No. 2, 1974, pp. 205–214.

[3] Sridhar, M. R., and Yovanovich, M. M., "Elastoplastic Contact Conductance Model for Isotropic Uniform Rough Surfaces and Comparison with Experiments," *Journal of Heat Transfer*, Vol. 118, Feb. 1996, pp. 3–9.

[4] Wahid, Syed M. S., and Madhusudana, C. V., "Gap Conductance in Contact Heat Transfer," *International Journal of Heat Transfer*, Vol. 43, No. 24, 2000, pp. 4483–4487.

[5] Yovanovich, M. M., Culham, J. R., and Teertstra, P., "Calculating Interface Resistance," *Electronics Cooling*, Vol. 3, No. 2, 1997, pp. 1–8.